New Tris(*tert*-butoxy)siloxy Complexes of Aluminum and Their Transformation to Homogeneous Aluminosilicate Materials via Low-Temperature Thermolytic Pathways

Claus G. Lugmair, Kyle L. Fujdala, and T. Don Tilley*

Department of Chemistry, University of California, Berkeley, Berkeley, California 94720-1460, and the Chemical Sciences Division, Lawrence Berkeley Laboratory, 1 Cyclotron Road, Berkeley, California 94720

Received September 10, 2001. Revised Manuscript Received November 13, 2001

The new tris(*tert*-butoxy)siloxy complexes of aluminum, Al[OSi(O^{t}Bu)$_3$]$_3$(THF) (**1**), Al[OSi(O^{t}Bu)$_3$]$_3$(HO^{i}Pr)·0.5[Al(O^{i}Pr)$_3$]$_4$ (**2**), and [(^{i}PrO)$_2$AlOSi(O^{t}Bu)$_3$]$_2$ (**3**), were synthesized. Compounds **2** and **3** were structurally characterized by single-crystal X-ray crystallography. Thermolysis of a toluene-d_8 solution containing **1** and 0.5 equiv of [Al(O^{i}Pr)$_3$]$_4$ resulted in the formation of **3** and free THF (by ^{1}H NMR spectroscopy). The low-temperature decompositions of **1**, **2**, and **3** allowed for their use as single-source precursors to high surface area aluminosilicate xerogels via solution (toluene) thermolyses. The DSC traces of the xerogels derived from the 1:1 Al/Si precursors (**2** and **3**) exhibited sharp exothermic transitions at ≈1000 °C, attributed to the crystallization of mullite, with that for the xerogel from **3** having a larger associated heat flow. The DSC trace of the xerogel derived from **1** exhibited a weak exothermic transition at a slightly higher temperature. Although these xerogels have similar ^{27}Al MAS NMR spectra, their microstructures appear to be quite different, as indicated by the substantially more efficient transformation to mullite (by PXRD) of the xerogel from **2**. All of the xerogels are homogeneous; however, the microstructure of the xerogel from **2** appears to more closely resemble that of mullite, given the enhanced formation of mullite (by PXRD) and the reduced free energy difference associated with mullite formation (by DSC). Acidity measurements characterized the Lewis/Brønsted site ratios as 1.2, 1.6, and 1.0 for the xerogels from **1**, **2**, and **3**, respectively.

Introduction

Aluminosilicates have been studied extensively as catalysts, catalyst supports, and structural materials.[1,2] Careful control of the microstructure of such materials is required to optimize their properties, and this is usually accomplished with low-temperature synthetic routes such as the sol−gel process. The formation of multicomponent oxides by the sol−gel process has typically been accomplished by matching the reactivities of various alkoxide precursors by chemical modification or by prehydrolysis of the less reactive precursor.[3] Alternatively, several groups have employed double-alkoxide precursors containing preformed Al−O−Si linkages in the preparation of aluminosilicate ceramics.[4−6] Such investigations by Pouxviel et al. focused on the hydrolysis of precursors such as (^{i}PrO)$_2$AlOSiMe$_3$ and (BuO)$_2$AlOSi(OEt)$_3$.[4] The Al−OR linkages in these precursors were found to be most susceptible to hydrolysis, while the Si−OEt and Si−Me groups were relatively unreactive. The initial stages of gel growth, therefore, involved the formation of Al−O−Al linkages, while longer gel times or more vigorous catalytic conditions were required for hydrolysis of the siloxide units.[4] In a related study, Ko and co-workers described the preparation of aluminosilicate aerogels with a 1:1 Si/Al ratio via two hydrolytic pathways. The first involved a standard sol−gel synthesis with prehydrolysis of the silica precursor. The second route involved the acid-catalyzed hydrolysis of a commercially available "double alkoxide", [(*sec*-BuO)$_2$AlOSi(OEt)$_3$]$_n$.[5]

(1) (a) Tanabe, K.; Misono, M.; Ono, Y.; Hattori, H. *New Solid Acids and Bases*; Elsevier: New York, 1989. (b) Subhash, B. *Zeolite Catalysis: Principles and Applications*; CRC Press: Boca Raton, FL, 1990. (c) *Zeolite Chemistry and Catalysis*; Jacobs, P. A., Jaeger, N. I., Kubelkova, L., Wichterlova, B., Eds.; Studies in Surface Science and Catalysis 69; Elsevier: New York, 1991. (d) Cauqui, M. A.; Rodríguez-Izquierdo *J. Non-Cryst. Solids* **1992**, *147−148*, 724.

(2) (a) *Mullite and Mullite Ceramics*; Schneider, H.; Okada, K.; Pask, J. A.; Wiley: New York, 1994. (b) *Mullite and Mullite Matrix Composites*; Somiya, S., Davis, R. F., Pask, J. A., Eds.; Ceramic Transactions Vol. 6; The American Ceramic Society: Westerville, OH, 1990.

(3) Brinker, C. J.; Scherer, G. W. *Sol−Gel Science*; Academic Press: Boston, 1990.

(4) (a) Pouxviel, J. C.; Boilot, J. P.; Dauger, A.; Huber, L. In *Better Ceramics Through Chemistry;* Brinker, C. J., Clark, D. E., Ulrich, D. R., Eds.; Materials Research Society Symposia Proceedings Vol. 73; Elsevier: New York, 1986; p 269. (b) Pouxviel, J. C.; Boilot, J. P.; Poncelet, O.; Hubert-Pfalzgraf, L. G.; Lecomte, A.; Dauger, A.; Beloeil, J. C. *J. Non-Cryst. Solids* **1987**, *93*, 277. (c) Pouxviel, J. C.; Boilot, J. P. In *Ultrastructure Processing of Advanced Ceramics*; Mackenzie, J. D., Ulrich, D. R., Eds.; Wiley: New York, 1988; p 197. (d) Chaput, F.; Lecomte, A.; Dauger, A.; Boilot, J. P. *Chem. Mater.* **1989**, *1*, 199.

(5) Miller, J. B.; Tabone, E. R.; Ko, E. I. *Langmuir* **1996**, *12*, 2878.

(6) (a) Williams, A. G.; Interrante, L. V. In *Better Ceramics Through Chemistry*; Brinker, C. J., Clark, D. E., Ulrich, D. R., Eds.; Materials Research Society Symposia Proceedings Vol. 32; North-Holland: New York, 1984; p 151. (b) Treadwell, D. R.; Dabbs, D. M.; Aksay, I. A. *Chem. Mater.* **1996**, *8*, 2056. (c) Andrianov, K. A.; Zhdanov, A. A. *J. Polym. Sci.* **1958**, *30*, 513. (d) Landry, C. C.; Davis, J. A.; Apblett, A. W.; Barron, A. R. *J. Mater. Chem.* **1993**, *3*, 597.

10.1021/cm010846h CCC: $22.00
Published on Web 01/22/2002

The crystallization of gel-derived aluminosilicate materials to mullite has been the subject of many investigations.[2,5,6b,7] The bulk composition of mullite is $3Al_2O_3 \cdot 2SiO_2$; however, a range of stoichiometries with $2.6 \leq Al/Si \leq 6.3$ that result from the substitution of Si with aluminum and incorporation of oxygen vacancies (eq 1) are associated with the mullite structure.[8] Poorly

$$2Si^{4+} + O^{2-} \leftrightarrow 2Al^{3+} + \text{vacancy} \quad (1)$$

homogeneous precursors such as mixtures of colloidal silica and alumina typically form a spinel phase between 980 and 1200 °C and then crystallize to mullite above ≈1250 °C.[7a,d] Highly homogeneous precursors exhibit a sharp exothermic transition in their DTA curves at ≈980 °C, above which crystalline mullite is observed.[7] The exothermic transition at 980 °C, associated with the crystallization of spinel or mullite, is believed to be initiated by the transformation of metastable pentacoordinate aluminum to tetrahedral and octahedral species.[9] The intensity of this peak was found to be the highest for highly homogeneous precursor mixtures and for precursors with a 3:1 Al/Si ratio.[7e] Higher silica contents were found to shift the exothermic transition to slightly higher temperatures.[7c]

We have been investigating metal complexes based on the $-OSi(O^tBu)_3$ ligand as single-source precursors to multicomponent oxide materials.[10] These complexes thermally decompose via the elimination of isobutene and water to form carbon-free homogeneous materials under very mild conditions (typically <200 °C). The thermolyses of these complexes in nonpolar solvents lead to the formation of gels that can be dried to form high surface area xerogels or aerogels, depending upon the method of drying. We have employed this *thermolytic molecular precursor* approach to generate a variety of metal−silicon−oxide materials with tailored properties.[10]

We previously reported synthesis of the aluminum siloxide precursors $[Me_2AlOSi(O^tBu)_3]_2$ and $[Me(^tBuO)AlOSi(O^tBu)_3]_3$ and their conversions to aluminosilicate materials.[10c,f] On the basis of these studies, we postulated that more efficient precursors might possess only Al−O and Si−O (and no Al−C) bonds. Aluminum−carbon bonds have been shown to enhance the thermal stability of the complexes and lead to solid-state materials with higher carbon contents.[10c,f] The study described here focuses on the synthesis of new tris(*tert*-butoxy)siloxy complexes of aluminum which can be used as single-source molecular precursors to aluminosilicate materials. The use of synthetic routes similar to those described by Abe and co-workers for the preparation of $\{(^iPrO)Al[OSi(O^tBu)_3]_2\}_2$[11] has resulted in isolation of the new species $Al[OSi(O^tBu)_3]_3(THF)$ (**1**), $Al[OSi(O^tBu)_3]_3(HO^iPr)\cdot 0.5[Al(O^iPr)_3]_4$ (**2**), and $[(^iPrO)_2AlOSi(O^tBu)_3]_2$ (**3**). The pyrolytic conversions of these complexes to generate high surface area aluminosilicate xerogels were carried out and the properties of these materials were examined.

Results and Discussion

Synthesis of the Aluminum Siloxides. The reaction of 12 equiv of $HOSi(O^tBu)_3$ with $[Al(O^iPr)_3]_4$ in refluxing THF formed $Al[OSi(O^tBu)_3]_3(THF)$ (**1**) in 72% yield (eq 2). Attempts to prepare this complex in higher

$$[Al(O^iPr)_3]_4 + 12HOSi(O^tBu)_3 \xrightarrow[-12HO^iPr]{\text{THF, 65 °C, 4 h}} 4Al[OSi(O^tBu)_3]_3(THF) \quad (2)$$

boiling noncoordinating solvents (such as benzene) led to the formation of a gel within 30 min. Complex **1** was also prepared from $[Al(O^tBu)_3]_2$ in THF; however, insoluble products were obtained when $[Al(OEt)_3]_4$ was used as the Al starting material. The ^1H NMR spectrum of **1** in benzene-d_6 reveals one resonance corresponding to the siloxide groups at 1.51 ppm and only one broad peak for the THF ligand (4.45 ppm). In $CDCl_3$, however, two sets of sharp resonances are observed for the THF ligand. Complex **1** is thermally unstable and decomposes to insoluble material over the course of a few weeks at room temperature. However, **1** may be stored for extended periods at −80 °C.

Abe and co-workers employed similar reactions in refluxing benzene to obtain a volatile complex with the empirical formula $(^iPrO)Al[OSi(O^tBu)_3]_2$, and their attempts to prepare an aluminum tris(siloxide) resulted in the formation of viscous gels.[11] We have previously noted the formation of a complex with one ^1H NMR resonance at 1.51 ppm, prepared from the reaction of Al_2Me_6 with excess $HOSi(O^tBu)_3$.[10c,f] This complex was postulated as an aluminum tris(siloxide); however, it was not isolated due to its thermal instability. The triphenylsiloxide analogue of **1**, $Al(OSiPh_3)_3(THF)$, which does not decompose until 353 °C, has been reported previously.[12]

(7) (a) Gerardin, C.; Sundaresan, S.; Benziger, J.; Navrotsky, A. *Chem. Mater.* **1994**, *6*, 160. (b) Yoldas, B. E. *J. Mater. Sci.* **1992**, *27*, 6667. (c) Hirata, Y.; Sakeda, K.; Matsushita, Y.; Shimada, K.; Ishihara, Y. *J. Am. Ceram. Soc.* **1989**, *72*, 995. (d) Yoldas, B. E.; Partlow, D. P. *J. Mater. Sci.* **1988**, *23*, 1895. (e) Okada, K.; Otsuka, N. *J. Am. Ceram. Soc.* **1986**, *69*, 652. (f) Parmentier, J.; Vilminot, S. *Chem. Mater.* **1997**, *9*, 1134. (g) Lin, C.; Ritter, J. A.; Amiridis, M. D. *J. Non-Cryst. Solids* **1997**, *215*, 146. (h) Klein, J.; Lettmann, C.; Maier, W. F. *J. Non-Cryst. Solids* **2001**, *282*, 203. (i) Takei, T.; Kameshima, Y.; Yasumori, A.; Okada, K.; Kumada, N.; Kinomura, N. *J. Non-Cryst. Solids* **2001**, *282*, 265. (j) McManus, J.; Ashbrook, S. E.; MacKenzie, K. J. D.; Wimperis, S. *J. Non-Cryst. Solids* **2001**, *282*, 278. (k) Takei, T.; Kameshima, Y.; Yasumori, A.; Okada, K. *J. Am. Ceram. Soc.* **1999**, *82*, 2876.

(8) (a) Cameron, W. E. *Am. Ceram. Soc. Bull.* **1977**, *56*, 1003. (b) Cameron, W. E. *Am. Miner.* **1977**, *62*, 747.

(9) Taylor, A.; Holland, D. *J. Non-Cryst. Solids* **1993**, *152*, 1.

(10) (a) McMullen, A. K.; Tilley, T. D.; Rheingold, A. L.; Geib, S. J. *Inorg. Chem.* **1989**, *28*, 3772. (b) McMullen, A. K.; Tilley, T. D.; Rheingold, A. L.; Geib, S. J. *Inorg. Chem.* **1990**, *29*, 2228. (c) Terry, K. W.; Tilley, T. D. *Chem. Mater.* **1991**, *3*, 1001. (d) Terry, K. W.; Gantzel, P. K.; Tilley, T. D. *Chem. Mater.* **1992**, *4*, 1290. (e) Terry, K. W.; Gantzel, P. K.; Tilley, T. D. *Inorg. Chem.* **1993**, *32*, 5402. (f) Terry, K. W. Ph.D. Thesis, University of California at San Diego, 1993. (g) Terry, K. W.; Lugmair, C. G.; Gantzel, P. K.; Tilley, T. D. *Chem. Mater.* **1996**, *8*, 274. (h) Su, K.; Tilley, T. D.; Sailor, M. J. *J. Am. Chem. Soc.* **1996**, *118*, 3459. (i) Su, K.; Tilley, T. D. *Chem. Mater.* **1997**, *9*, 588. (j) Terry, K. W.; Lugmair, C. G.; Tilley, T. D. *J. Am. Chem. Soc.* **1997**, *119*, 9745. (k) Rulkens, R.; Tilley, T. D. *J. Am. Chem. Soc.* **1998**, *120*, 9959. (l) Lugmair, C. G.; Tilley, T. D. *Inorg. Chem.* **1998**, *37*, 764. (m) Terry, K. W.; Su, K.; Tilley, T. D.; Rheingold, A. L. *Polyhedron* **1998**, *17*, 891. (n) Rulkens, R. R.; Male, J. L.; Terry, K. W.; Olthof, B.; Khodakov, A.; Bell, A. T.; Iglesia, E.; Tilley, T. D. *Chem. Mater.* **1999**, *11*, 2966. (o) Coles, M. P.; Lugmair, C. G.; Terry, K. W.; Tilley, T. D. *Chem. Mater.* **2000**, *12*, 122. (p) Male, J. L.; Niessen, H. G.; Bell, A. T.; Tilley, T. D. *J. Catal.* **2000**, *194*, 431. (q) Kriesel, J. W.; Tilley, T. D. *J. Mater. Chem.* **2001**, *11*, 1081. (r) Fujdala, K. L.; Tilley, T. D. *Chem. Mater.* **2001**, *13*, 1817. (s) Fujdala, K. L.; Tilley, T. D. *J. Am. Chem. Soc.* **2001**, *123*, 10133.

(11) Kijima, I.; Yamamoto, T.; Abe, Y. *Bull. Chem. Soc. Jpn.* **1971**, *44*, 3193.

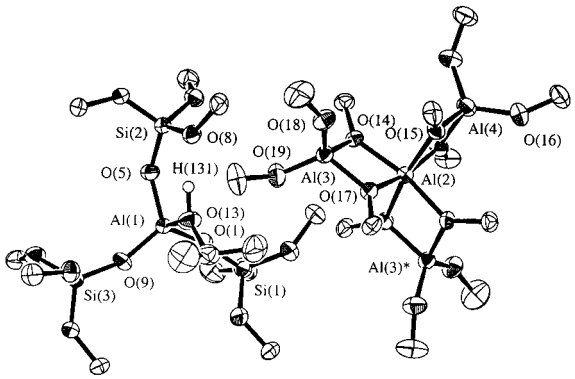

Figure 1. ORTEP view of the molecular structure of Al[OSi(O^{t}Bu)$_3$]$_3$(HO^{i}Pr)·$^1/_2$[Al(O^{i}Pr)$_3$]$_4$ (**2**). The methyl groups have been removed for clarity. Thermal ellipsoids have been drawn to 50% probability.

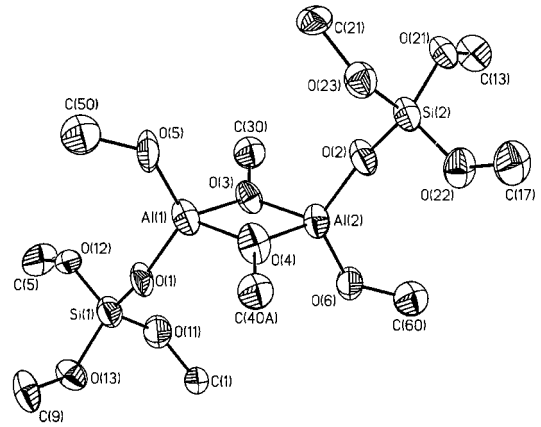

Figure 2. Thermal ellipsoid plot (50% probability) of [(O^{i}Pr)$_2$AlOSi(O^{t}Bu)$_3$]$_2$ (**3**). The methyl groups, hydrogen atoms, and one disordered methine carbon on each isopropyl group have been removed for clarity.

An attempt was made to prepare a precursor with a higher aluminum content (Al/Si ratio of 1:1) by heating a mixture of [Al(O^{i}Pr)$_3$]$_4$ and 4 equiv of HOSi(O^{t}Bu)$_3$ to reflux in hexanes. This resulted in formation of a fully substituted aluminum tris(siloxide), Al[OSi(O^{t}Bu)$_3$]$_3$(HO^{i}Pr), which cocrystallized from the reaction mixture with unreacted [Al(O^{i}Pr)$_3$]$_4$, hence yielding **2** in 95% yield (eq 3). Thus, crystals of **2** possess Al and Si in a

$$3[Al(O^iPr)_3]_4 + 12HOSi(O^tBu)_3 \xrightarrow[-8HO^iPr]{\text{hexanes, 60 °C, 2 h}} 4Al[OSi(O^tBu)_3]_3(HO^iPr)\cdot{}^1/_2[Al(O^iPr)_3]_4 \quad (3)$$
$$\mathbf{2}$$

1:1 ratio, and this stoichiometry does not change after several recrystallizations. A single-crystal X-ray study of **2** was performed to unequivocally determine the molecular composition and the structure of the Al[OSi(O^{t}Bu)$_3$]$_3$(HO^{i}Pr) component (Figure 1).

A further attempt was made to form an aluminum monosiloxide complex by thermal redistribution of the ligands in the mixture of compounds denoted as **2**. However, heating an octane solution of **2** at 126 °C resulted in the formation of a viscous gel within 15 min. In contrast, when [Al(O^{i}Pr)$_3$]$_4$ and 2 equiv of **1** were heated at 120 °C in isooctane for 5 h, the new aluminum siloxide complex [(O^{i}PrO)$_2$AlOSi(O^{t}Bu)$_3$]$_2$ (**3**) was obtained in 44% yield (eq 4). This complex was found to thermally

$$2Al[OSi(O^tBu)_3]_3(THF) + [Al(O^iPr)_3]_4 \xrightarrow[-2THF]{\text{isooctane, 120 °C, 5 h}} 3[(^iPrO)_2AlOSi(O^tBu)_3]_2 \quad (4)$$
$$\mathbf{1} \qquad\qquad \mathbf{3}$$

decompose at room temperature in the solid state and in solution over the course of a few days. A solution molecular weight determination of **3** by the Singer mehod[13] was hindered by this decomposition. Interestingly, the reaction of [Al(O^{i}Pr)$_3$]$_4$ with 4 equiv of HOSi(O^{t}Bu)$_3$ in toluene at 80 °C also yielded **3**, although the yield was quite low (30%). The dimeric structure of **3** was established by single-crystal X-ray crystallography (Figure 2).

A potentially key difference between the reaction conditions leading to **2** and **3** is the identity of the datively coordinated ligand of the tris(siloxide) complex (THF or HO^{i}Pr). We assume that HO^{i}Pr promotes decomposition of the AlOSi species present in solution. Indeed, the decomposition of metal tris(*tert*-butoxy)siloxy complexes is known to be Brønsted acid catalyzed.[10j] It is interesting to note that the use of toluene in the reaction of [Al(O^{i}Pr)$_3$]$_4$ with 4 equiv of HOSi(O^{t}Bu)$_3$ gives rise to a 1:1 complex, whereas the isolation of only a 1:3 Al/Si complex was possible from THF or hexanes. Thus, subtle solvent effects appear to play an important role in the syntheses of these aluminum siloxides.

Single-Crystal X-ray Structures of 2 and 3. The asymmetric unit of **2** contains a complete Al[OSi(O^{t}Bu)$_3$]$_3$(HO^{i}Pr) complex and one-half of an [Al(O^{i}Pr)$_3$]$_4$ tetramer while that of **3** contains 1.5 molecules of [(O^{i}Pr)$_2$AlOSi(O^{t}Bu)$_2$]$_2$. Despite exhaustive attempts at crystallization, the crystals of **3** were of poor quality and contained a mirror twin normal to the *c* axis, thus limiting the resolution to 1.1 Å. The Al−OSi bond distances in the tris(siloxide) component of **2** range from 1.693(2) to 1.721(2) Å and those in **3** range from 1.684(6) to 1.694(6) Å. The HO^{i}Pr ligand in **2** is oriented such that the hydroxyl proton is directed toward O(8), and the O(8)−O(13) distance of 2.670(3) Å indicates the presence of hydrogen bonding. As a result of this hydrogen-bonding interaction, the siloxide ligand containing O(8) is significantly distorted. The metrical parameters of the [Al(O^{i}Pr)$_3$]$_4$ complex in **2** agree very closely with those obtained from a crystal structure analysis of pure [Al(O^{i}Pr)$_3$]$_4$.[14] In general, the analogous bond distances and angles in **3** and in the Al[OSi(O^{t}Bu)$_3$]$_3$(HO^{i}Pr) portion of **2** are similar. The crystallographic data for **2** and **3** are summarized in Table 1 and selected bond distances and angles are given in Tables 2 and 3 for **2** and **3**, respectively.

Thermolytic Behavior of 1−3 in the Solid State. Thermogravimetric analysis (TGA) revealed that **1**

(12) Apblett, A. W.; Warren, A. C.; Barron, A. R. *Can. J. Chem.* **1992**, *70*, 771.

(13) (a) Signer, R. *Leibigs Ann. Chem.* **1930**, *478*, 246. (b) Zoellner, R. W. *J. Chem. Educ.* **1990**, *67*, 714.

(14) Folting, K.; Streib, W. E.; Caulton, K. G.; Poncelet, O.; Hubert-Pfalzgraf, L. G. *Polyhedron* **1991**, *10*, 1639.

Table 1. Crystallographic Data for Complexes 1 and 2

	$Al[OSi(O^tBu)_3(HO^iPr)\cdot {}^1/_2[Al(O^iPr)_3]_4$ (**2**)	$[(O^iPr)_2AlOSi(O^tBu)_3]_2$ (**3**)[a]
formula (asymmetric unit)	$C_{51}H_{131}Al_3O_{19}Si_3$	$C_{34}H_{123}Al_3O_{18}Si_3$
crystal system	monoclinic	monoclinic
space group	*C*2	$P2_1/c$
Z	4	4
cell constants		
a (Å)	23.989(1)	9.097(3)
b (Å)	13.9207(7)	24.530(7)
c (Å)	23.902(1)	33.678(10)
β (deg)	95.349(1)	90.205(6)
V (Å^3)	7953.2(6)	7515.2(39)
D_{calc} (g cm^{-3})	1.365	1.083
μ (Mo Kα) (cm^{-1})	1.9	1.5
radiation	Mo Kα (0.70169 Å)	Mo Kα (0.70169 Å)
scan type	ω (0.3°/frame)	ω (0.3°/frame)
temperature (°C)	−110	−112
exposure time	30 s/frame	30 s/frame
measured reflections	16870	34230
unique reflections	10992	24139
residuals:		
	$R(F) = 0.039$	$R(F^2) = 0.055$
	$R(wF) = 0.048$	$R(wF^2) = 0.089$
	GOF = 2.06	GOF = 0.84
max./min. peak in the difference map (e Å^{-3})	0.39; −0.22	0.27; −0.26

[a] The asymmetric unit contains 1.5 molecules of **3**.

decomposes at a low temperature (Figure 3a), with an onset to decomposition at ≈95 °C. At 1000 °C the ceramic yield (26.7%) was slightly lower than the expected ceramic yield of 28.3% for $^1/_2Al_2O_3\cdot 3SiO_2$. Complex **1** does not melt prior to decomposition. The initial volatile decomposition products obtained by heating a solid-state sample of **1** at 155 °C for 10 min were collected by vacuum transfer and quantified by ^{1}H NMR spectroscopy, using ferrocene as a standard, in benzene-d_6. The products were isobutene (5.8 equiv), HO^{t}Bu (0.93 equiv), HOSi(O^{t}Bu)$_3$ (0.11 equiv), H_2O (0.7 equiv), and THF (0.64 equiv).

The mixture of complexes denoted as **2** also decomposes at a low temperature, with an onset to decomposition at ≈138 °C (Figure 3b). There was no indication of a two-step decomposition as might be expected for a physical mixture of two compounds. At 1000 °C the ceramic yield (25.7%) was very close to the expected ceramic yield of 25.9% for $^3/_2Al_2O_3\cdot 3SiO_2$. Crystals of **2** soften at 80 °C and melt at 116 °C, close to the reported melting point of pure $[Al(O^iPr)_3]_4$ (118 °C).[15] The initial volatile decomposition products obtained by thermolysis of **2** at 180 °C for 10 min were propene (0.41 equiv), isobutene (2.16 equiv), HO^{i}Pr (1.6 equiv), HO^{t}Bu (0.49 equiv), and HOSi(O^{t}Bu)$_3$ (0.03 equiv).

Unfortunately, the instability of complex **3** prevented us from obtaining meaningful TGA data; however, the solid appears to become a sticky mass at 110 °C and liquifies at ≈130 °C. Decomposition appeared to be occurring throughout the entire heating process, as evident by a continuous loss of mass.

Hydrolytic Behavior of the Aluminum Siloxides. To characterize the hydrolytic stabilities of the aluminum siloxide complexes, their interactions with small quantities (1 equiv) of water were monitored by solution ^{1}H NMR spectroscopy. A gel rapidly formed upon addition of water to a benzene-d_6 solution of **1**. The resulting mixture contained unreacted **1**, free THF, and HOSi(O^{t}Bu)$_3$. Some new siloxide resonances, presumably corresponding to partially hydrolyzed aluminum siloxide species, also appeared in the ^{1}H NMR spectrum near the resonance for **1**. Hydrolysis of **2** with 1 equiv of water in benzene-d_6 produced HO^{i}Pr and HOSi(O^{t}Bu)$_3$ in a 2.8/1 ratio. This indicates that the hydrolysis of Al−O−Si linkages in **1** is competitive with hydrolysis of Al−O^{i}Pr linkages in $[Al(O^iPr)_3]_4$. The ^{1}H NMR spectrum also contained resonances for both complexes in **2** as well as some new siloxide resonances. In contrast, the hydrolysis of **3** in benzene-d_6 with 1 equiv of water produced primarily HO^{i}Pr with only small amounts of HOSi(O^{t}Bu)$_3$. Several new siloxide resonances were also observed. In the above hydrolysis experiments, HO^{t}Bu was not detected. This reflects the hydrolytic stability of HOSi(O^{t}Bu)$_3$.

Solution Thermolyses of the Aluminum Siloxides. The solution-phase thermolytic decompositions of the aluminum siloxide precursors were monitored as a function of time. Toluene-d_8 solutions of the precursor and a known amount of ferrocene, as standard, were sealed in an NMR tube. The sample was then placed in a preheated NMR probe. The concentrations of the starting materials as well as the decomposition products were then monitored over time.

The decomposition of **1** was examined at 70 °C (Figure 4a). After ≈2000 s, the concentration of isobutene began to slowly increase. After ≈3800 s a sudden decomposition occurred, indicated by the rapid disappearance of **1** and a concomitant increase in the concentrations of isobutene and HO^{t}Bu. During the decomposition a small amount of HOSi(O^{t}Bu)$_3$ appeared, which also rapidly decomposed to isobutene and HO^{t}Bu. It is interesting to note that the first "hydrolysis product" that is formed is HOSi(O^{t}Bu)$_3$ and only after most of the starting material has been consumed does HO^{t}Bu appear. Also, the aluminosilicate gel that is formed during the reaction is an efficient catalyst for the decomposition of HOSi(O^{t}Bu)$_3$ since the pure silanol is indefinitely stable at this temperature. What is not clear, however, is how much of the decomposition occurs via the HOSi(O^{t}Bu)$_3$ intermediate. Although the concentration of the silanol is quite low at any given time, significant quantities of it may form during the reaction, as it would be continuously converted to isobutene and HO^{t}Bu. Regardless, the growing inorganic network presumably retains the Al-to-Si ratio of the precursor because of the immediate decomposition of the silanol.

The thermolysis of a toluene-d_8 solution containing **1** and 0.5 equiv of $[Al(O^iPr)_3]_4$ was monitored at 140 °C (Figure 4b). Within the first 5 min of the thermolysis, resonances corresponding to **3** and free THF appear. Three small resonances also appeared very close to the siloxide resonance of **3**. Because of their similar chemical shifts, all resonances corresponding to aluminum siloxide species were integrated together and all resonances corresponding to aluminum isopropoxide species were integrated together. Surprisingly, no HOSi(O^{t}Bu)$_3$ was detected at any time during the thermolysis. The

(15) (a) Shiner, V. J.; Whittaker, D.; Fernandez, V. P. *J. Am. Chem. Soc.* **1963**, *85*, 2318. (b) Mehrotra, R. C. *J. Ind. Chem. Soc.* **1954**, *31*, 85.

Table 2. Selected Bond Distances (Å) and Angles (deg) for 2[a]

		Distances			
Si(1)−O(1)	1.579(2)	Si(2)−O(7)	1.622(2)	Al(1)−O(1)	1.698(2)
Si(1)−O(2)	1.621(2)	Si(2)−O(8)	1.655(2)	Al(1)−O(5)	1.721(2)
Si(1)−O(3)	1.623(3)	Si(3)−O(9)	1.594(2)	Al(1)−O(9)	1.693(2)
Si(1)−O(4)	1.623(2)	Si(3)−O(10)	1.622(2)	Al(1)−O(13)	1.853(2)
Si(2)−O(5)	1.593(2)	Si(3)−O(11)	1.625(2)	O(8)−H(131)	1.64
Si(2)−O(6)	1.617(2)	Si(3)−O(12)	1.621(2)	O(13)−H(131)	1.09
		Angles			
O(1)−Si(1)−O(2)	106.8(1)	O(6)−Si(2)−O(7)	107.4(1)	O(1)−Al(1)−O(5)	113.9(1)
O(1)−Si(1)−O(3)	111.7(1)	O(6)−Si(2)−O(8)	104.7(1)	O(1)−Al(1)−O(9)	113.9(1)
O(1)−Si(1)−O(4)	113.7(1)	O(7)−Si(2)−O(8)	111.6(1)	O(1)−Al(1)−O(13)	105.8(1)
O(2)−Si(1)−O(3)	113.5(1)	O(9)−Si(3)−O(10)	114.1(1)	O(5)−Al(1)−O(9)	117.2(1)
O(2)−Si(1)−O(4)	105.1(1)	O(9)−Si(3)−O(11)	106.2(1)	O(5)−Al(1)−O(13)	96.3(1)
O(3)−Si(1)−O(4)	106.0(1)	O(9)−Si(3)−O(12)	112.2(1)	O(9)−Al(1)−O(13)	106.9(1)
O(5)−Si(2)−O(6)	115.4(1)	O(10)−Si(3)−O(11)	106.6(1)	Si(1)−O(1)−Al(1)	158.7(1)
O(5)−Si(2)−O(7)	112.3(1)	O(10)−Si(3)−O(12)	105.9(1)	Si(2)−O(5)−Al(1)	141.4(1)
O(5)−Si(2)−O(8)	104.7(1)	O(11)−Si(3)−O(12)	111.8(1)	Si(3)−O(9)−Al(1)	159.2(2)

[a] Only parameters for the $Al[OSi(O^tBu)_3]_3 \cdot (HO^iPr)$ portion of the structure are given.

Table 3. Selected Bond Distances (Å) and Angles (deg) for 3[a]

		Distances			
Si(1)−O(1)	1.588(6)	Si(2)−O(22)	1.608(7)	Al(1)−O(4)	1.812(6)
Si(1)−O(12)	1.616(7)	Si(2)−O(23)	1.620(7)	Al(1)−O(5)	1.670(7)
Si(1)−O(13)	1.621(6)	Si(2)−O(21)	1.633(7)	Al(2)−O(6)	1.658(6)
Si(1)−O(11)	1.635(7)	Al(1)−O(1)	1.687(6)	Al(2)−O(2)	1.684(6)
Si(2)−O(2)	1.596(6)	Al(1)−O(3)	1.815(7)	Al(2)−O(3)	1.799(7)
				Al(2)−O(4)	1.827(6)
		Angles			
O(1)−Si(1)−O(12)	106.7(4)	O(22)−Si(2)−O(21)	114.3(3)	O(6)−Al(2)−O(3)	112.3(3)
O(1)−Si(1)−O(13)	112.0(3)	O(23)−Si(2)−O(21)	106.6(4)	O(2)−Al(2)−O(3)	111.8(3)
O(12)−Si(1)−O(13)	113.5(4)	O(5)−Al(1)−O(1)	119.1(3)	O(6)−Al(2)−O(4)	112.0(3)
O(1)−Si(1)−O(11)	112.8(3)	O(5)−Al(1)−O(4)	112.1(4)	O(2)−Al(2)−O(4)	114.3(3)
O(12)−Si(1)−O(11)	106.1(4)	O(1)−Al(1)−O(4)	111.3(3)	O(3)−Al(2)−O(4)	81.3(3)
O(13)−Si(1)−O(11)	105.7(4)	O(5)−Al(1)−O(3)	112.3(4)	Si(1)−O(1)−Al(1)	148.7(4)
O(2)−Si(2)−O(22)	105.4(4)	O(1)−Al(1)−O(3)	114.6(3)	Si(2)−O(2)−Al(2)	149.8(4)
O(2)−Si(2)−O(23)	112.3(3)	O(4)−Al(1)−O(3)	81.2(3)	Al(2)−O(3)−Al(1)	99.2(3)
O(22)−Si(2)−O(23)	106.5(4)	O(6)−Al(2)−O(2)	119.1(3)	Al(1)−O(4)−Al(2)	98.3(3)
O(2)−Si(2)−O(21)	111.8(4)				

[a] Values are for the full molecule of **3** in the asymmetric unit, as shown in Figure 2.

concentration of aluminum isopropoxide species decreased more rapidly than the concentration of aluminum siloxide species. After ≈4900 s the decomposition became rapid and both of these species disappeared quickly. The organic portions of the siloxide ligands were converted primarily to isobutene and small amounts of HO^tBu. The concentration of HO^tBu reached a maximum during the rapid phase of the decomposition (at ≈4900 s) and then decreased, indicating that it was dehydrated to isobutene under the reaction conditions. The isopropoxide ligands were converted primarily to HO^iPr. Only small amounts of propene, presumably from the dehydration of HO^iPr, were observed at the end of the reaction. The similar rates for the elimination of O^iPr and O^tBu ligands during the solution thermolysis of **3** (by ^1H NMR spectroscopy) imply that both Si and Al may be incorporated into the growing gel network simultaneously to maximize the efficient formation of Al−O−Si linkages.

Aluminosilicate Xerogels from 1 to 3. The low temperature at which the aluminum siloxide precursors thermally decompose to carbon-free inorganic species allows these pyrolysis reactions to be conducted in organic solvents. Xerogels were prepared in toluene from **1**, **2**, and a mixture of **1** with 0.5 equiv of $[Al(O^iPr)_3]_4$. It was anticipated that **3** would form in situ from the mixture of **1** with 0.5 equiv of $[Al(O^iPr)_3]_4$ in the early stages of the thermolyses, as observed in the NMR studies described above.

Heating a toluene solution of **1** to 110 °C resulted in the formation of a clear gel within 10 min. Transparent xerogel pieces (≈5 mm^3) remained after air-drying the wet gel for 2 days. The xerogel was further dried under N_2 at 150 °C for 12 h and then calcined at 500 °C under O_2 for 2 h. After this heat treatment the sample contained 0.22% carbon and 1.89% hydrogen (by combustion analysis). Elemental analysis also revealed that the Al/Si ratio in this xerogel was 1:2.95, indicating that the stoichiometry of the precursor is maintained upon conversion to the material. This material had a BET surface area of 531 $m^2\ g^{-1}$ and a pore volume of 0.57 $cm^3\ g^{-1}$. The N_2 adsorption−desorption isotherm is shown in Figure 5a. The shape of the isotherm, classified as type IV, arises from capillary condensation of an adsorbate inside a mesoporous solid.[16] The hysteresis between the adsorption isotherm (lower curve) and the desorption isotherm (upper curve) is classified as type H2[16] (type E in earlier literature[17]), which is generally believed to arise from condensation in solids that are comprised of loosely packed spherical particles.[18] The pores in these types of materials are thought to consist of large cavities that are accessible only through narrow

(16) Sing, K. S. W.; Everett, D. H.; Haul, R. A. W.; Moscou, L.; Pierotti, R. A.; Rouqerol, J.; Siemieniewska, T. *Pure Appl. Chem.* **1985**, *57*, 603.

(17) Lowell, S.; Shields, J. E. *Powder Surface Area and Porosity*; Chapman and Hall: New York, 1984.

(18) Lecloux, A. J. In *Catalysis Science and Technology*, Anderson, R. J.; Boudart, M. Eds.; Springer-Verlag: New York, 1981; p 171.

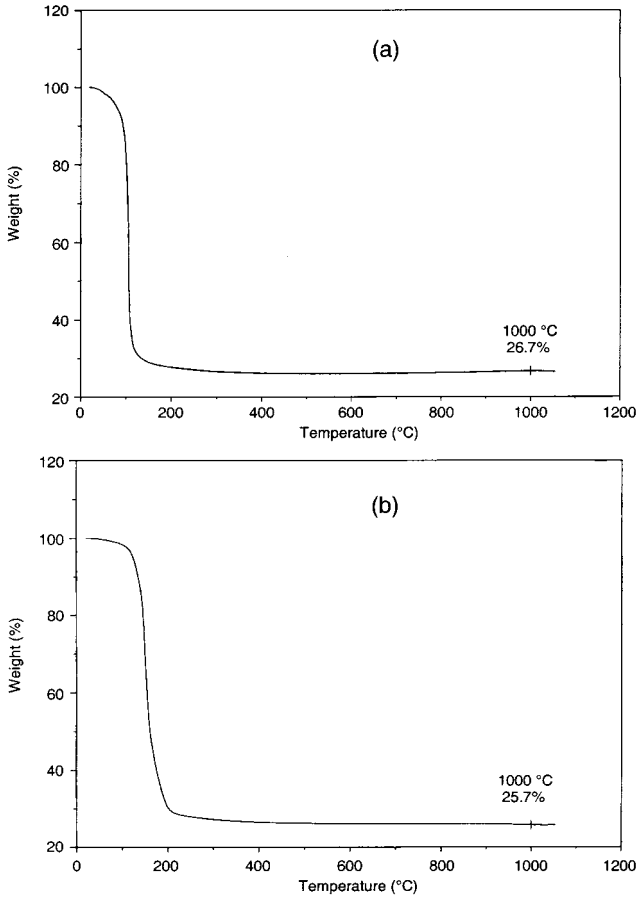

Figure 3. TGA traces in N_2 with a heating rate of 10 °C min^{-1} for (a) **1** and (b) **2**.

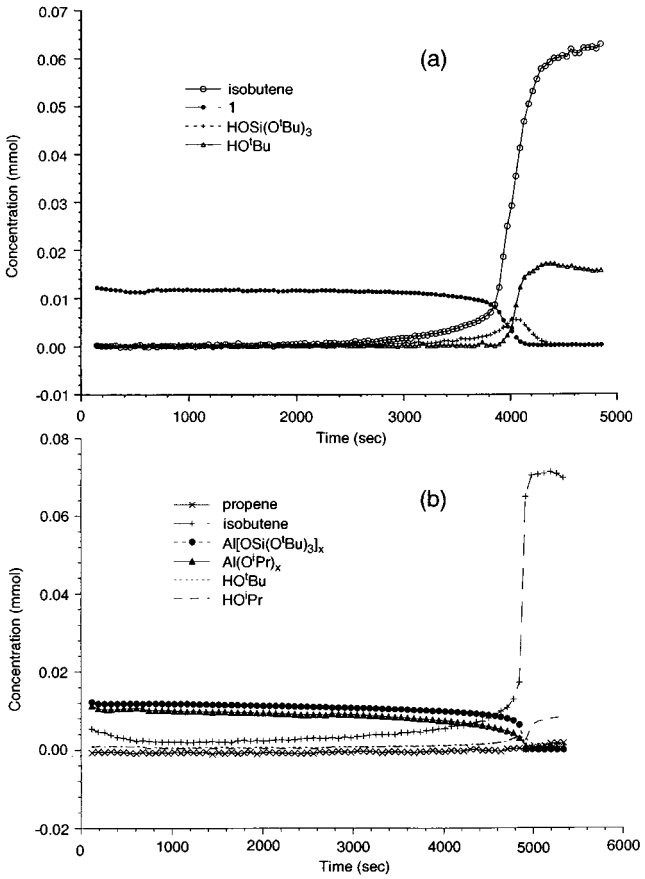

Figure 4. (a) Plot showing the concentrations of **1** and its major decomposition products as a function of time. The thermolysis of **1** was performed at 70 °C in toluene-d_8. (b) Plot of the temporal evolution of the thermolysis of a mixture of 2 equiv of **1** and $[Al(O^iPr)_3]_4$ in toluene-d_8 at 140 °C. The curves marked $Al[OSi(O^tBu)_3]_x$ and $Al(O^iPr)_x$ represent the integrated intensity of all resonances corresponding to aluminum siloxides and aluminum isopropoxides, respectively.

necks; however, it is now recognized that this model may be an oversimplification.[16] The average pore diameter in this xerogel was 44 Å. The pore size distribution, as calculated from the adsorption isotherm, shows that there are a large number of small mesopores (≈20 Å) and steadily fewer pores as the pore diameter increases (Figure 5b). A transmission electron microscope (TEM) image of the xerogel calcined at 500 °C shows that this material consists of fine primary particles ≤5 nm.

The crystallization behavior of the xerogel from **1** was probed by differential scanning calorimetry (DSC), which revealed a small exothermic transition that exhibited a broad peak at ≈1024 °C with an associated heat flow of 15 J g^{-1} (Figure 6a). A powder X-ray diffraction (PXRD) pattern of the xerogel, calcined at 1100 °C, shows very weak reflections corresponding to mullite (Figure 7a). Thus, the mild exothermic event in the DSC trace may be attributed to the crystallization of a small amount of mullite.

A gel was also prepared from the mixture denoted as **2** by heating a toluene solution of the precursor to 145 °C for 12 h. The resulting clear gel was air-dried for 10 days and further dried under N_2 at 100 °C for 12 h. This xerogel had a BET surface area of 583 m^2 g^{-1}. A sample calcined at 500 °C under O_2 for 2 h contained 0.14% carbon and 2.26% hydrogen (by combustion analysis). Elemental analysis of this xerogel determined the Al/Si ratio to be 1:1.03, indicating that the stoichiometry of **2** is retained in the material that is formed after solution thermolysis. The DSC trace of the xerogel exhibits an exothermic event at 1001 °C (43 J g^{-1}), attributed to the crystallization of mullite (Figure 6b). The xerogel remains amorphous after heating to 900 °C under O_2 as shown by PXRD (Figure 7b). Further heating to 1000 °C resulted in the crystallization of mullite with an average crystallite size of 18 nm (estimated by the Scherrer equation).[19] No exothermic transitions were observed between 1200 and 1300 °C, which would be indicative of mullite crystallization from poorly homogeneous mixtures.

Thermolysis of a toluene solution containing **1** + $^1/_2[Al(O^iPr)_3]_4$ (to form **3** in situ) at 110 °C resulted in the formation of a gel within 12 h. The gel was air-dried for 10 days and then calcined at 500 °C under O_2. After this heat treatment the sample contained 0.22% carbon and 1.65% hydrogen (by combustion analysis). Elemental analysis revealed the Al/Si ratio to be 0.90:1.0, indicating approximate incorporation of all Si and Al from **3**. This calcined xerogel had a BET surface area of 226 m^2 g^{-1} and a pore volume of 0.27 cm^3 g^{-1}. The average pore diameter was 49 Å. The N_2 adsorption−desorption isotherm of this xerogel (Figure 8a) was also of type IV with a type H2 hysteresis. This indicates that the xerogel consists of an assembly of spherical particles.[16] The pore size distribution calculated from the

(19) Scherrer, P. *Nachr. Ges. Wiss. Göttingen* **1918**, 96.

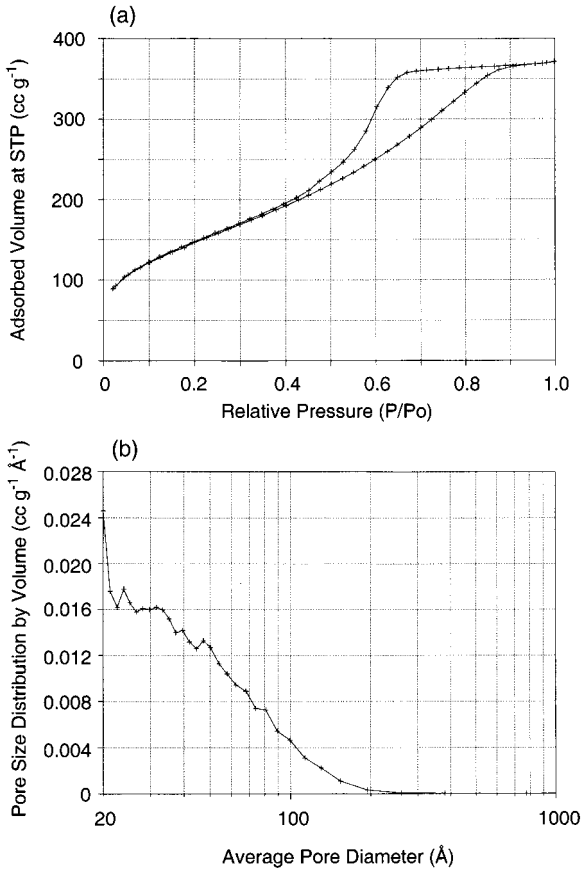

Figure 5. N_2 adsorption−desorption isotherms (a) and the pore size distribution calculated from the adsorption data (b) for the xerogel from **1** after calcination at 500 °C in O_2.

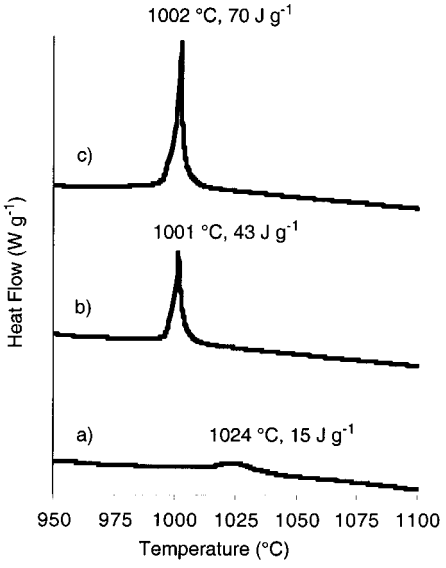

Figure 6. Differential scanning calorimetry (DSC) traces of the aluminosilicate materials: (a) xerogel from **1**, (b) xerogel from **2**, and (c) xerogel from **3**.

adsorption isotherm (Figure 8b) exhibits a maximum at ≈40 Å with few small mesopores and a negligible number of pores with a diameter above 110 Å. This material consists of larger primary particles (4−19 nm) than the xerogel from **1** (by TEM).

The DSC trace for the xerogel from **3** revealed a sharp exotherm at 1002 °C (70 J g^{-1}) corresponding to the crystallization of mullite (Figure 6c). No phase transitions were observed at higher temperature. The xerogel remained amorphous by PXRD after heating to 1000 °C (Figure 7c). Crystalline mullite with an average particle size of 23 nm was present after heating to 1100 °C. The mullite crystallites are not clearly visible by TEM presumably because of the similar density of mullite and the amorphous matrix.

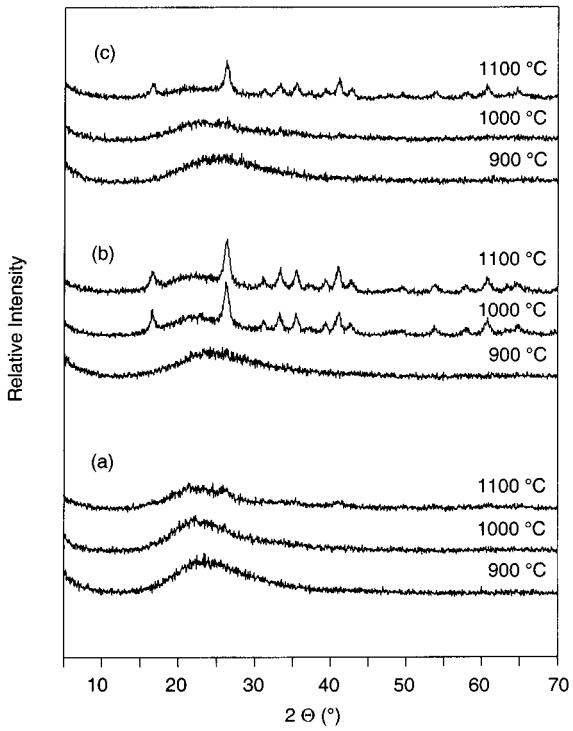

Figure 7. Powder X-ray diffraction patterns of the xerogels prepared from (a) **1**, (b) **2**, and (c) a mixture of **1** with 0.5 equiv of $[Al(O^iPr)_3]_4$ (to form **3** in situ) calcined at 900, 1000, and 1100 °C in O_2.

The crystallizations of mullite from the xerogels derived from the 1:1 Si/Al precursors (**2** and **1** + $^1/_2[Al(O^iPr)_3]_4$) are both marked by sharp exothermic transitions in their DSC curves near 1000 °C. The heat flow associated with this exothermic event was 1.5 times greater for the xerogel derived from **3**. An intense peak in the differential thermal analysis (DTA) trace (a related measurement) for the crystallization of mullite has been interpreted as stemming from high degrees of atomic-scale mixing in the premullite ceramic.[5,7a,b,d] This interpretation implicates the xerogel derived from complex **3** (formed in situ from **1** + $^1/_2[Al(O^iPr)_3]_4$) as being the most homogeneous of the samples examined here. In contrast to these results, however, the xerogel from **3** (calcined at 1100 °C) contains relatively poorly developed mullite crystallites (by PXRD) compared to the xerogel from **2**. For comparison, Ko and co-workers' double-alkoxide hydrolytically derived gel exhibits well-formed mullite crystallites (by PXRD) after a similar heat treatment.[5] The greater extent of crystallization determined by PXRD has also been interpreted as arising from a highly homogeneous sample.[5,7a,b,d,i,k] Thus, the PXRD and DSC results for the 1:1 Si/Al precursors seem to be contradictory. Resolution of the apparent inconsistency between the PXRD and DSC data will undoubtedly require a more detailed understanding of the intimate microstructure of these premullite ceramics.

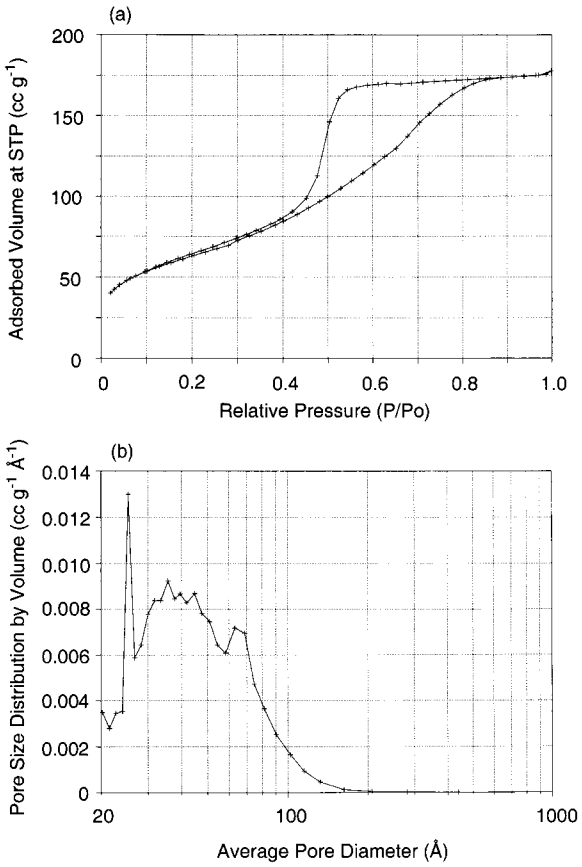

Figure 8. N_2 adsorption−desorption isotherms (a) and the pore size distribution calculated from the adsorption data (b) for the xerogel prepared from a mixture of **1** with 0.5 equiv of $[Al(O^iPr)_3]_4$ (to form **3** in situ) after calcination at 500 °C in O_2.

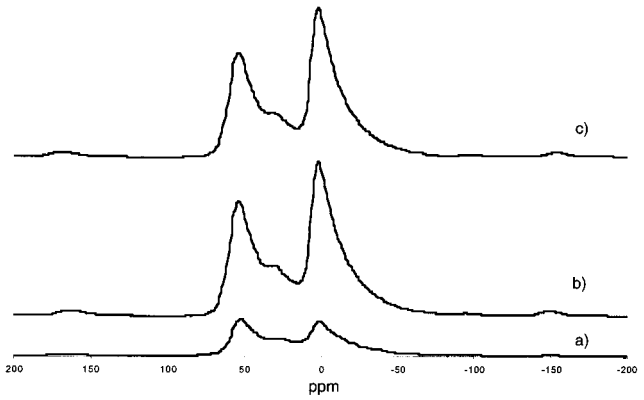

Figure 9. ^{27}Al MAS NMR spectra of the calcined xerogels (500 °C in O_2) prepared from (a) **1**, (b) **2**, and (c) **3**.

^{27}Al MAS NMR Spectroscopy. Solid-state ^{27}Al magic-angle spinning (MAS) NMR analysis of the xerogel from **1** after calcination at 500 °C revealed resonances centered at ≈53, 29, and 2 ppm (Figure 9a). These peaks correspond to four-, five-, and six-coordinate Al species, respectively.[20] It has also been suggested that peaks at ≈30 ppm in aluminosilicates may be due to severely distorted four-coordinate Al sites with a weakly coordinated oxygen atom or to four-coordinate Al tricluster sites.[20d] The ^{27}Al MAS NMR analyses of the xerogels from **2** and **3** after calcination at 500 °C revealed four-, five-, and six-coordinate Al as indicated by peak positions of ≈55, 32, and 3 ppm, respectively (Figure 9b,c).

Qualitatively, the spectra of the xerogels from **2** and **3** are nearly identical in terms of peak positions and relative peak intensities, with the peak corresponding to six-coordinate Al being slightly more intense than that for four-coordinate Al. This is in contrast to the xerogel obtained from **1**, for which the peak corresponding to four-coordinate Al is more intense. The similarity of the spectra for **2** and **3** suggests similar local environments for the Al species; however, the broadness of the peaks in the ^{27}Al MAS NMR spectra is indicative of the existence of many environments. Hence, subtle differences between samples may not be discernible.

Table 4. Acidity Data for the Aluminosilicate Samples after Calcination at 500 °C in O_2

sample (Al/Si ratio)	total acid site concn (sites nm^{-2})[b]	OH concn (sites nm^{-2})[c]	Lewis acid concn (sites nm^{-2})[d]	Lewis/ Brønsted site ratio
xerogel from **1** (1:3)	2.8 ± 0.4	1.3 ± 0.2	1.5 ± 0.4	1.2
xerogel from **2** (1:1)	2.1 ± 0.4	0.8 ± 0.2	1.3 ± 0.4	1.6
xerogel from **3**[a] (1:1)	4.7 ± 0.4	2.3 ± 0.2	2.4 ± 0.4	1.0
SBA-15	1.0 ± 0.1	1.0 ± 0.1	0	N/A

[a] From the thermolysis of a mixture of **1** and 0.5 equiv of $[Al(O^iPr)_3]_4$. [b] Determined from NH_3 TPD experiments (monitored by TGA). Errors are based on 2σ (95% confidence level) as determined from 5 to 10 measurements. [c] Determined from reaction of the sample with $Mg(CH_2Ph)_2$·2THF (monitored by ^{1}H NMR spectroscopy). Errors are based on 2σ as determined from the integration of 5−10 ^{1}H NMR spectra monitored over the course of several hours. [d] Determined by difference.

Determination of Acid Site Coverages. The temperature-programmed desorption (TPD) of ammonia (monitored by TGA) was used to determine the total acid site concentration in the aluminosilicate xerogels after calcination at 500 °C.[21] The concentration of Brønsted acid (OH) sites was determined by quantifying the amount of toluene evolved after the reaction of the aluminosilicate materials with $Mg(CH_2Ph)_2$·2THF.[10s] Table 4 provides a summary of the results of these measurements. It is apparent that the xerogel obtained from the thermolysis of **3** has the highest concentration of Brønsted sites and that from **2** has the lowest. For comparison, similar measurements were performed on the mesoporous silica material SBA-15.[22]

Studies of the hydrolysis and condensation of double-alkoxide precursors indicate that polymeric networks containing Al−O−Al linkages form first followed by condensation of a silica network.[4] Such a microstructure may be envisioned as a bicontinuous network of inter-

(20) (a) Engelhardt, G.; Michel, D. *High-Resolution Solid-State NMR Of Silicates and Zeolites*; John Wiley & Sons: New York, 1987. (b) Okada, K.; Tomita, T.; Kameshima, Y.; Yasumori, A.; MacKenzie, K. J. D. *J. Mater. Chem.* **1999**, *9*, 1307. (c) Sánchez-Soto, P. J.; Pérez-Rodríguez, J. L.; Sobrados, I.; Sanz, J. *Chem. Mater.* **1997**, *9*, 677. (d) McManus, J.; Ashbrook, S. E.; MacKenzie, K. J. D.; Wimperis, S. *J. Non-Cryst. Solids* **2001**, *282*, 278 and references therein.

(21) Selected references for NH_3 TPD of related materials: (a) Miyamoto, Y.; Katada, N.; Niwa, M. *Microporous Mesoporous Mater.* **2000**, *40*, 271. (b) Kosslick, H.; Lischke, G.; Parlitz, B.; Storek, W.; Fricke, R. *Appl. Catal. A* **1999**, *184*, 49. (c) Gagnasco, G. *J. Catal.* **1996**, *159*, 249. (d) Toba, M.; Mizukami, F.; Niwa, S.; Sano, T.; Maeda, K.; Shoji, H. *J. Mater. Chem.* **1994**, *4*, 1131. (e) Chen, C. Y.; Li, H. X.; Davis, M. E. *Microporous Mater.* **1993**, *2*, 17.

(22) Zhao, D. Y.; Feng, J. L.; Huo, Q. S.; Melosh, N.; Fredrickson, G. H.; Chmelka, B. F.; Stucky, G. D. *Science* **1998**, *279*, 548.

twined alumina and silica polymers. Brønsted acid sites in aluminosilicate materials typically arise from AlO_x polyhedra surrounded exclusively by SiO_4 tetrahedra.[1a] A higher ratio of Lewis/Brønsted acid sites (1.6) in the xerogel from **2** suggests that more Al−O−Al linkages may be present as compared to the xerogel derived from **3** (with a Lewis/Brønsted ratio of 1.0). This might be expected due to the presence of $[Al(O^iPr)_3]_4$, which contains preformed Al−O−Al linkages, in the mixture denoted as **2**. Ko and co-workers reported a Lewis/Brønsted site ratio of 2.6 for their aerogel derived hydrolytically from a double alkoxide,[5] supporting previous studies showing that alumina networks form prior to silica condensation during gel synthesis by the hydrolysis of double alkoxides.[4] The formation of Lewis acid sites is enhanced as amorphous aluminosilicates obtain microstructures closer to that of mullite.[23] Although not an efficient premullite ceramic, the xerogel derived from **1** has a relatively low Lewis/Brønsted site ratio (1.2), as expected for an aluminosilicate that is silicon-rich.[1]

Concluding Remarks

The single-source precursors **1**, **2**, and **3** are well-suited for producing homogeneous carbon-free aluminosilicate materials with retention of the Al/Si ratio. Indeed, the solution-phase thermolyses of **1**, **2**, and **1** + $^1/_2[Al(O^iPr)_3]_4$ (to form **3** in situ) produced xerogels with small spherical particles and high surface areas that are attractive as potential solid acid catalysts and as catalyst supports. Silica xerogels with a similar texture have previously been obtained by two-step sol−gel preparations involving an acid-catalyzed step followed by a base-catalyzed step.[3] The solution-phase thermolysis of each precursor occurs at a low temperature and leads to the simultaneous incorporation of Al and Si into the growing gel network. The materials prepared in this manner have a moderate degree of surface Brønsted acidity, making them potentially well-suited for catalytic applications.[1a,d] In addition, the 1:1 Si/Al aluminosilicate materials derived from **2** and **3** transform to mullite at low temperatures (≈1000 °C), indicating that they are homogeneous. The efficiency of the transformation to mullite is similar to that of Ko and co-workers' 1:1 Si/Al materials obtained by sol−gel routes involving the hydrolysis of a double alkoxide or the prehydrolysis of a silicon-containing precursor followed by the cohydrolysis of an aluminum-containing precursor.[5] The behavior of **3** upon partial hydrolysis is similar to what has been observed for the hydrolysis of other double alkoxides.[4−6]

It is evident that the aluminosilicate ceramics derived from **1**, **2**, and **3** are highly homogeneous, yet they possess distinctly different microstructures. Thus, interpretation of the intensity of the exotherm in DSC or DTA curves associated with mullite crystallization in amorphous aluminosilicates as arising solely from the degree of "atomic-scale mixing" in the premullite ceramic appears to be an oversimplification. A higher degree of homogeneity of the premullite ceramic should require minimal diffusion for the crystallization of mullite. Thus, from a homogeneous sample a greater amount of mullite will crystallize during the exothermic event near 1000 °C, leading to a large peak in the DSC or DTA curve. If the amorphous ceramic not only is homogeneous but also has a microstructure that is very similar to that found in crystalline mullite, the free energy difference between the amorphous premullite ceramic and crystalline mullite should be small. Although such a premullite ceramic should lead to the crystallization of a large amount of mullite, the small free energy change upon crystallization should result in a smaller peak in the DSC or DTA trace. Therefore, when comparing the crystallization behavior of atomically well-mixed premullite aluminosilicate ceramics, the exothermicity of the crystallization does not necessarily parallel the degree of crystallization.

Fewer Brønsted sites nm^{-2}, a less energetic DSC transition for the formation of mullite, and the presence of larger mullite crystallites in the PXRD diffractogram for the xerogel derived from **2** indicate that its microstructure is closer to that of mullite than is that of the xerogel derived from **3**. The preexistence of Al−O−Al linkages in the $[Al(O^iPr)_3]_4$ unit in the mixture of compounds denoted as **2** appears to lead to more of these linkages in the final material, as might be expected. Hence, the xerogel derived from the true single-source molecular precursor (**3**) appears to have a more even distribution of Al and Si with fewer Al−O−Al domains. It is clear that seemingly subtle differences in the microstructure of amorphous aluminosilicate materials have dramatic effects on their properties, specifically their crystallization behavior and surface acidities. It would seem that, for the most efficient transformation to mullite, an amorphous aluminosilicate must possess a high degree of homogeneity and have a microstructure that closely resembles that of mullite.

Experimental Details

All manipulations were performed under a nitrogen atmosphere using standard Schlenk techniques or a Vacuum Atmospheres drybox unless otherwise noted. Diethyl ether, tetrahydrofuran, and pentane were distilled from sodium benzophenone under nitrogen. Toluene and benzene were distilled from sodium under nitrogen and then degassed. Solution NMR spectra were recorded on a Bruker AMX-300 spectrometer at 300 (^{1}H) or 75.5 (^{13}C) MHz or on a Bruker AMX-400 spectrometer at 400 (^{1}H) or 100 (^{13}C) MHz. Benzene-d_6 and toluene-d_8 were vacuum-transferred from a Na/K alloy, and $CDCl_3$ was vacuum-transferred from CaH_2. Solid-state ^{27}Al magic-angle spinning (MAS) NMR spectra were recorded on a Chemagnetics CMX 400 spectrometer operating at a frequency of 104.3 MHz. The samples were loaded into a 4-mm ZrO_2 rotor and spun at the magic angle with a rate from 15.5 to 16.5 kHz. The ^{27}Al MAS spectra were obtained with a 1-μs pulse length (nonselective $\pi/2$ of 6 μs), a relaxation delay of 0.1 s, and a digitization rate of 500 kHz. Measurements were collected at room temperature and the peak positions are reported relative to $[Al(H_2O)_6]^{3+}$. Infrared spectra were collected as Nujol mulls on a Mattson galaxy 3000 spectrometer, using CsI cells. Thermolyses were performed using a Lindberg 1700 °C or a Lindberg 1200 °C three-zone tube furnace. Heat treatments were carried out in flowing (500 cm^3 min^{-1}) nitrogen (99.98%) or oxygen (99.96%). Transmission electron microscopy was performed on a JEOL 100CX microscope. Thermal analyses were performed on a DuPont model 2000 thermal analysis system (TGA) or on a TA Instruments SDT 2960 integrated TGA/DSC thermal analyzer (DSC). Ammonia TPD experiments were performed using a TA Instruments SDT 2960 integrated TGA/DSC thermal analyzer. Powder X-ray diffraction data were collected on a Siemens D5000

(23) Sundaresen, S.; Aksay, I. A. *J. Am. Ceram. Soc.* **1991**, *74*, 2388.

spectrometer using Cu Kα radiation. Surface area and pore volume measurements were performed on a Quantachrome Autosorb surface area analyzer. Elemental analyses were performed by Galbraith Analytics, Knoxville, TN, and Desert Analytics, Tuscon, AZ. The compound $[Al(O^iPr)_3]_4$ was purchased from Aldrich and purified by distillation. The compounds $[Al(OEt)_3]_4$,[24] $[Al(O^tBu)_2]_2$,[24] and $HOSi(O^tBu)_3$[10f,25] and SBA-15[22] were prepared according to literature procedures.

$Al[OSi(O^tBu)_3]_3(THF)$ (1). To a solid mixture of $[Al(O^iPr)_3]_4$ (1.91 g, 2.33 mmol) and $HOSi(O^tBu)_3$ (7.43 g, 28.1 mmol) was added THF (50 mL). The reaction mixture was heated to reflux for 4 h. The solvent was then removed in vacuo and the remaining white solid was extracted into pentane (30 mL). The solution was filtered, concentrated to 15 mL, and cooled (−40 °C), affording 6.02 g of **1** as colorless crystals in 72% yield.

$Al[OSi(O^tBu)_3]_3(^iPrOH)\cdot{}^1/_2[Al(O^iPr)_3]_4$ (2). To a solid mixture of $[Al(O^iPr)_3]_4$ (4.28 g, 5.23 mmol) and $HOSi(O^tBu)_3$ (5.54 g, 20.9 mmol) was added hexane (30 mL). The reaction mixture was sealed in a 100-mL vessel and heated to 60 °C for 2 h. The solvent was then removed in vacuo and the remaining white solid was extracted into hexane (30 mL). The solution was filtered, concentrated to 10 mL, and cooled (−40 °C), affording 8.07 g of **2** as colorless crystals in 95% yield.

$[(^iPrO)_2AlOSi(O^tBu)_3]_2$ (3). (a) To a solid mixture of $[Al(O^iPr)_3]_4$ (0.117 g, 0.143 mmol) and **1** (0.235 g, 0.575 mmol) was added isooctane (40 mL). The reaction mixture was sealed in a 100-mL vessel and heated to 120 °C for 5 h. The solvent was then removed in vacuo and the remaining oily solid was extracted into pentane (30 mL). The solution was filtered, concentrated to 10 mL, and cooled (−80 °C) to afford 0.155 g of **3** as colorless crystals in 44% yield.

(b) Complex **3** was also prepared from the reaction of $[Al(O^iPr)_3]_4$ (0.692 g, 0.720 mmol) with $HOSi(O^tBu)_3$ (0.762 g, 2.90 mmol) in toluene at 80 °C. The toluene (5 mL) was added to a solid mixture of the reagents in a Schlenk tube under N_2. The Schlenk tube containing the resulting clear and colorless solution was heated at 80 °C for 18 h in an oil bath with magnetic stirring. The reaction mixture remained clear and colorless throughout the heating period. The solvent was removed in vacuo, leaving a colorless solid. The solid was dissolved in toluene, MeCN was added (to give a 2:1 toluene: MeCN mixture), and the resulting clear solution was stored at −30 °C for 24 h. Colorless crystals were obtained and washed with acetonitrile, yielding analytically pure **3** as an opaque solid in 30% yield (0.353 g). Insoluble material precipitated out of the mother liquor upon continued storage at −30 °C. Complex **3** could not be stored for extended periods without the formation of insoluble material resulting from its decomposition.

Thermolysis of 1 in Solution. A toluene solution (10 mL) of **1** (1.5 g, 1.84 mmol) was sealed in a 100-mL flask with a PTFE valve. The flask was submerged in an oil bath that had been preheated to 110 °C. After 10 min a clear gel formed that filled the entire volume that the solution originally occupied. Heating was continued for an additional 12 h. The flask was then allowed to cool and the small amount of excess solvent was decanted. The wet gel was allowed to air-dry for 2 days, yielding transparent xerogel pieces ≈5 mm^3 in size.

Thermolysis of 2 in Solution. A toluene solution (10 mL) of **2** (8.0 g, 6.22 mmol) was sealed in a 100-mL Pyrex ampule. The ampule was placed in an oven that had been preheated to 145 °C. After 12 h a clear gel formed that filled the entire volume that the solution originally occupied. The ampule was cooled to room temperature and opened, and the gel was allowed to air-dry over 10 days.

Thermolysis of 1 and $[Al(O^iPr)_3]_4$ in Solution. A toluene solution (10 mL) of **1** (1.0 g, 1.22 mmol) and $[Al(O^iPr)_3]_4$ (0.50 g, 0.61 mmol) was sealed in a 100-mL flask with a PTFE valve. The flask was submerged in an oil bath that had been preheated to 110 °C. After 12 h a clear gel formed that filled the entire volume that the solution originally occupied. The flask was allowed to cool and the excess solvent was decanted. The wet gel was allowed to air-dry for 10 days, yielding a transparent xerogel.

Temperature-Programmed Desorption of Ammonia. Typical TPD measurements were performed as follows: The sample to be analyzed was loaded into the furnace of an integrated TGA/DSC (TA Instruments SDT 2960), using Pt sample and reference pans. The mass of each sample was typically between 20 and 30 mg (measured in situ after initial thermal treatment). The sample was calcined in O_2 (100 mL min^{-1}) at 500 °C for 1 h and then at 500 °C in N_2 (100 mL min^{-1}) for an additional 1 h. The furnace was cooled to 40 °C in flowing N_2 and immediately dosed with 1% NH_3 in He (flowing at 100 mL min^{-1}) for 1 h. After the 1-h dosing period at 40 °C the furnace was immediately purged with N_2 for 1 h (100 mL min^{-1}) to remove the excess NH_3 (at 40 °C). The loss of mass on N_2 purging leveled off after between 30 and 50 min (typical weight losses on purging ranged from 0.3 to 0.5%). The temperature was then ramped at 10 °C min^{-1} in N_2 to 500 °C. The temperature was maintained at 500 °C for 1 h to ensure that complete loss of NH_3 had occurred (typically, no change in mass was observed for longer than 30 min at 500 °C). The furnace was then cooled to 40 °C, immediately dosed with NH_3, and treated as previously described. Samples were treated in this fashion for 5−10 consecutive runs to allow for the determination of error (2σ was used for error, giving a 95% confidence level). No air exposure occurred throughout the entire series of runs.

The mass of the sample was monitored throughout the entire run to record the mass of adsorbed NH_3, the mass loss upon purging, and the mass loss from desorption with heating. Only the mass loss from desorption with heating was used for acid site determinations. Control runs with no NH_3 dosing period revealed that small amounts of N_2 were taken up by the sample; however, it was assumed that the NH_3 would displace any adsorbed N_2 during the dosing period. Typical mass losses for desorption upon heating ranged from 2.895 to 4.660% (of the total mass) for the aluminosiicate xerogels and from 2.009 to 2.356% for SBA-15. No significant variation in the amount of NH_3 desorbed was observed when different heating rates were used (i.e., 2 °C min^{-1}). The total number of acid sites in a given sample was determined by using the mass loss of NH_3 upon heating to calculate the number of moles of NH_3 and then converting to the number of molecules of NH_3 (to give the number of sites per *sample*, assuming that one NH_3 occupies one site). The total surface area of the *sample* (in nm^2) was used to calculate the acid site concentration (sites nm^{-2}).

Determination of OH Site Coverage. Typical determinations of the OH content of each sample were performed as follows: The material was calcined at 500 °C in O_2 (100 mL min^{-1}) for 2 h, transferred to a Schlenk tube, heated in vacuo at 120 °C for ≈24 h, and brought into a drybox for preparation. A J-Young NMR tube was charged with the material to be analyzed (from 10.0 to 20.0 mg), a measured amount of ferrocene (from 8.0 to 15.0 mg), and a measured amount of $Mg(CH_2Ph)_2\cdot 2THF$ (from 10.0 to 20.0 mg) in a drybox. The sample tube was evacuated (using a Schlenk line with a vacuum-transfer apparatus) and benzene-d_6 was transferred into the sample tube (cooled with $N_2(l)$) under reduced pressure. The sample tube was warmed to room temperature and was then agitated for a period of time (typically 10 min). The ^1H NMR spectrum was then recorded at room temperature.

A series of spectra were recorded over the course of several hours until the reaction was deemed complete. The amount of CH_3Ph formed from the reaction of $Mg(CH_2Ph)_2$ and the OH groups of the solid material was measured by integration against the ferrocene standard using the cleanly resolved methyl resonance of the toluene. Between 5 and 10 spectra were recorded for each sample to allow for determination of the error (2σ−95% confidence level). It should be noted that the disappearance of $Mg(CH_2Ph)_2\cdot 2THF$ is not a reliable measure of the OH content of the sample because of potential reactivity with the solid material (i.e., reaction at Lewis sites).

(24) Bradley, D. C.; Mehrotra, R. C.; Gaur, D. P. *Metal Alkoxides*; Academic Press: New York, 1978.

(25) Abe, Y.; Kijima, I. *Bull. Chem. Soc. Jpn.* **1969**, *42*, 1118.

It should also be noted that only OH sites that are accessible to the $Mg(CH_2Ph)_2$ reagent will be detected; hence, the measurement may result in an underestimation due to OH sites confined within small pores. Test runs of the material in benzene-d_6 and ferrocene with no $Mg(CH_2Ph)_2 \cdot 2THF$ did not produce any toluene. The ^1H NMR spectrum of $Mg(CH_2Ph)_2 \cdot 2THF$ in benzene-d_6 also did not show the presence of toluene. The total number of OH sites in a given sample was determined by calculating the number of moles of toluene produced (relative to the ferrocene standard) and converting to the number of molecules of toluene (to give the number of sites per *sample*). The total surface area of the *sample* (in nm^2) was then used to calculate the OH site density (sites nm^{-2}).

Crystallographic Structure Determinations of 2 and 3. Crystals of **2** suitable for X-ray analysis were grown from a concentrated pentane solution that was stored at −80 °C and crystals of **3** were grown from a mixture of toluene and acetonitrile (5:1) at −30 °C. A colorless blocky crystal of **2** with dimensions of 0.30 × 0.30 × 0.30 mm or a thin fragment of a colorless platelike crystal having dimensions of 0.30 × 0.15 × 0.05 mm was mounted on a glass fiber using Paratone N hydrocarbon oil. Data were collected using a Siemens SMART diffractometer with a CCD area detector. A preliminary orientation matrix and unit cell parameters of **2** were determined by collecting 60 10-s frames, followed by spot integration and least-squares refinement. Cell constants and an orientation matrix for **3** were obtained from a least-squares refinement using the measured positions of 1872 reflections in the range $3.00° < 2\theta < 45°$. The data were collected at a temperature of -110 ± 1 and −112 °C for **2** and **3**, respectively. Frames corresponding to an arbitrary hemisphere of data were collected using ω scans of 0.3° and a collection time of 30 s/frame. Frame data were integrated using SAINT (SAX Area-Detector Integration Program; V4.024; Siemens Industrial Automation, Inc.: Madison, WI, 1995). The data were corrected for Lorentz and polarization effects. An empirical absorption correction for **2** was performed using XPREP (part of the SHELXTL Crystal Structure Determination Package; V5.03; Siemens Industrial Automation, Inc.: Madison, WI, 1995) ($\mu = 0.19$ mm^{-1}, $T_{max} = 0.93$, $T_{min} = 0.86$) and that for **3** was performed using SADABS (Siemens Area Detector Absorption Corrections; Sheldrick, G. M., 1996) ($\mu = 0.15$ mm^{-1}, $T_{max} = 0.98$, $T_{min} = 0.66$). The 16 870 integrated reflections for **2** were averaged in point group 2/*m* to give 10 992 unique reflections ($R_{int} = 0.022$). Of these, 9647 reflections were considered observed ($I > 3.00\sigma(I)$). Inspection of the systematic absences uniquely defined the space group *C*2. The 34 230 integrated reflections for **3** were averaged to give 24 139 unique reflections ($R_{int} = 0.123$). Of these, 3225 reflections were considered observed ($I > 2\sigma(I)$). The crystal system was determined to be monoclinic and the space group found to be $P2_1/c$. No decay correction was necessary in either case.

The structure of **2** was solved using direct methods (SIR92), expanded using Fourier techniques (DIRDIF92), and refined by full-matrix least-squares methods using teXsan software (Crystal Structure Analysis Package, Molecular Structure Corporation, 1985 & 1992). The structure of **3** was solved using direct methods and expanded using Fourier techniques by using the SHELXTL suite of programs (Sheldrick, G. M. SHELXTL, V5.03; Seimens Crystallographic Research Systems: Madison, WI, 1994). The non-hydrogen atoms of **2** were refined anisotropically. A peak was found in a Fourier difference map that was in a chemically reasonable position for the hydroxyl proton H(131) on O(13). A hydrogen atom was included at this position but not refined. The remaining hydrogen atoms in **2** were included at calculated positions but not refined. Inversion of the structure did not lead to an improvement in the *R* factor. The number of variable parameters was 738, giving a data/parameter ratio of 13.07. The maximum and minimum peaks on the final difference Fourier map corresponded to 0.38 and −0.21 $e^-/Å^3$. Residuals (*F*): $R = 0.039$, $R_w = 0.047$, and GOF = 2.05.

The data for **3** rapidly decreased in intensity with $\sin\theta/\lambda$. This, coupled with a β angle close to 90°, indicated the potential for mirror twinning normal to *a* or *c*. Inspection of the structure and unit cell indicated that the mirror twin was normal to *c*. An appropriate twin law (100 010 00−1) was applied and the twin occupancy refined (62:38). Some of the O^{t}Bu methyl groups were disordered and modeled with 50% occupancy over two sites. The ^{i}Pr groups were similarly disordered, with the carbon atoms modeled over two positions at 50% occupancy as either split (due to large thermal motion) or as two atoms at the same position, with equal thermal parameters (to accommodate the calculation of the appropriate number of hydrogen atoms). The Al, Si, O, and nondisordered C atoms were refined anisotropically, the disordered C atoms were refined isotropically, and the H atoms were added as fixed contributors at calculated positions with thermal parameters based upon the C atom to which they were bonded. The final cycle of full-matrix least-squares refinement (on F^2) was based on 3225 reflections ($I > 2\sigma(I)$) and 650 variable parameters (data/parameter ratio = 5.0) and converged with unweighted and weighted agreement factors of $R_{obs} = 0.055$, $wR_2 = 0.089$, $R_{all} = 0.146$, and $GOF_{all} = 0.84$, $GOF_{obs} = 1.05$. The maximum and minimum peaks on the final difference Fourier map corresponded to 0.27 and −0.26 $e^-/Å^3$.

Acknowledgment. This work was supported by the Director, Office of Energy Research, Office of Basic Energy Sciences, Chemical Sciences Division, of the U.S. Department of Energy under Contract DE-AC03-76SF00098. We thank B. L. Phillips at Univeristy of California, Davis, for the MAS NMR spectra and A. M. Stacey for the use of instrumentation (PXRD).

Supporting Information Available: NMR, EA, and IR data for **1**, **2**, and **3**, tables of crystal data, data collection, and refinement parameters, bond distances and angles, and anisotropic displacement parameters for **2** and **3** (PDF). This material is available free of charge via the Internet at http://pubs.acs.org.

CM010846H